Biomass Conversion and Biorefinery (2024) 14:31369–31381
https://doi.org/10.1007/s13399-023-04786-6

ORIGINAL ARTICLE

Production of Si-doped biomass-derived materials: effect of support type, activation and doping conditions

Nurgül Özbay[1] · Adife Şeyda Yargıç[1] · Elif Yaman[2] · Rahmiye Zerrin Yarbay[1] · Kamil Burak Dermenci[3] · Servet Turan[3]

Received: 28 June 2023 / Revised: 14 August 2023 / Accepted: 20 August 2023 / Published online: 29 August 2023

Abstract

Biomass-based carbonaceous materials have a great deal of promise for usage as anode material in lithium-ion batteries, which are one of the safest and most energy-dense energy storage technologies. The scientific community has assigned considerable focus on sustainable carbon production methods because of their low cost and eco-friendly features. Sustainable materials were produced as a result of selecting the renewable resource, and it also contributed to waste management since the feedstock was furniture industry waste. Herein, it was aimed to produce silicon-doped carbonaceous materials under different activation and doping conditions by using biomass and biochar support. Spruce wood sawdust, which had a carbon content of 46.55 wt.%, lignin content of 35.21 wt.%, and lower ash content (1.41 wt.%), was a suitable raw material to be evaluated by the pyrolysis method. Since the highest char yield was achieved in the pyrolysis reactions performed at 400 °C, silicon-doping experiments were executed with the biochar sample obtained at this temperature. Acidic and alkaline activations were applied to samples to specify the impacts of various activation conditions on the characteristics of the silicon-doped carbonaceous materials. In order to examine the effect of doping conditions on the crystalline structure, the reaction medium was changed to air and nitrogen. The produced silicon-doped carbon materials were characterized using Fourier Transform Infrared Spectroscopy (FT-IR), X-Ray Diffraction (XRD), Scanning Electron Microscopy (SEM), Energy Dispersive X-Ray Spectroscopy (EDX) and EDX-mapping techniques. According to the characterization results, no crystalline silicon peaks were observed in the sample produced at 700 °C, 8 h. The porous structure of the biochar was preserved in each synthesis condition and silicon was homogeneously distributed in the carbon structure. The highest silicon content of 27.43% was obtained as a result of applying the heating process at 550 °C for 6 h after silicon loading to the biomass. The preparation of silicon-doped porous carbonaceous materials from spruce sawdust and char via thermochemical and chemical methods with appropriate properties reveals an important potential in terms of evaluating them in supercapacitors, which are among the developing electrochemical energy stores.

Keywords Biomass · Biochar · Activation · Silicon · Carbonaceous materials

1 Introduction

Global energy needs, contemporary environmental contamination, and global warming are major ecological problems caused by the advancement of technology. The conversion of renewable sources, specifically biomass, may be a promising solution to this issue. Being an organic substance, biomass is formed from the wastes of living organisms like plants and animals. Plants, waste materials [1], and wood [2] all known as biomass resources, are the most frequently utilized biomass feedstocks for energy. The fact that biomass cannot be consumed like fossil fuels is just one of its numerous advantages. Biomass could become a crucial renewable energy source that can sustainably replace fossil

✉ Nurgül Özbay
nurgul.ozbay@bilecik.edu.tr

[1] Department of Chemical Engineering, Bilecik Şeyh Edebali University, 11100 Bilecik, Turkey

[2] Department of Alternative Energy Resources Technology, Vocational School, Bilecik Şeyh Edebali University, 11100 Bilecik, Turkey

[3] Department of Materials Science and Engineering, Eskisehir Technical University, 26555 Eskisehir, Turkey

fuels because there are plenty of plants on Earth [3]. Typically, biomass primarily contains cellulose, hemicelluloses, and lignin, as also starches, proteins, minerals, oils, nucleic acids, and resins. Cellulose predominates in a significant portion of plant-derived biomass, whereas lignin prevails in woody biomass. The range of cellulose content in biomass is between 40 and 60 wt.%. About 20–40 weight percent of biomass is composed of hemicelluloses, which are comparatively less stable [4]. The biomass source can differ based on the qualities and potential of a specific biomass to transform it into a valuable energy source or to utilize it as another type of material, including biochar.

A cost-effective, effective, and environmentally friendly method for accomplishing sustainable development objectives is biochar usage, a carbonaceous solid byproduct from the pyrolysis of biomass. In recent decades, numerous porous biochars with perfect quality from biomass (such as leaves, fruits, coconut shells, fibers, and husk) have been produced [5]. This method involves first carbonizing the lignocellulosic biomass materials to remove all the undesired volatile components before being thermally decomposed at a high temperature to achieve the desired porous carbon product [1]. The characteristics of the biochar produced by biomass pyrolysis directly affect the subsequent char activation stage because the quantity and type of pores control the gas accessibility to the active surface sites. The activation step of biochar can be investigated in two groups chemical and physical activation. In the physical activation, biochar synthesized from biomass is heated to a temperature higher than 700 °C in a stream of hot steam or CO_2 gas, or both. In the chemical activation, the biomass/biochar is treated with an acid, alkali, or salt solution. The most commonly used chemical activation agents can be listed as phosphoric acid (H_3PO_4), sulfuric acid (H_2SO_4), zinc chloride ($ZnCl_2$), potassium hydroxide (KOH), sodium hydroxide (NaOH), and ferric chloride ($FeCl_3$). The kind of activating agents has a significant impact on both the chemical activation mechanism and the properties of the derived product. Two processes take place in the phosphoric acid activation: first, depolymerizing lignin, hemicellulose, and cellulose while promoting the formation of crosslinks between carbon polymers within dehydration and condensation reactions; second, encouraging the development of phosphate and polyphosphate that bridge and further crosslink the biopolymer fragments produced by the first step. Phosphate groups facilitate a dilation mechanism that generates an easily accessible porous matrix once the acid has been removed. The activation with potassium hydroxide, on the contrary, primarily entails the fragmentation and solubilization of substances in biomass by a reduction reaction while causing potassium-including atoms inside the carbon network. The porosity of the carbon structure is enhanced by these and other potassium component species, which are incorporated within the carbon network and finally eliminated during pyrolysis and washing [6]. Chemical activation method is more advantageous than physical activation as it provides higher activation efficiency. In addition, the carbon yield is higher, higher porosity biochar is obtained [7], it needs a shorter reaction time and lower reaction temperature [8]. Wastewater treatment, precursor catalysts [1], the catalyst for diverse chemical conversions for bio-oil or biodiesel production [9], soil additives including fertilizer, adsorption of hazardous substances, and energy storage [10] are all applications for biochar.

The development of energy storage technologies based on innovative, clean, and high-efficiency materials, such as supercapacitors, is required due to the rise of the oil crisis and environmental damage prompted by the combustion of fossil fuels [11]. With the increasing importance of electric vehicles, the interest in lithium-ion batteries has also increased. The commercial graphite anode's (372 mAh g^{-1}) restricted capacity cannot meet the requirements for implementations that require high energy density. Thus, the fabrication of materials with greater specific capacities is required. Among them, silicon has promise as a lithium-ion battery anode material. The volume expansion of silicon during application causes the electrode material to be crushed, negatively affecting the performance of Li-ion batteries. In order to eliminate this disadvantage of silicon, combining silicon with carbon materials has been presented as a solution [12]. With the production of hybrid materials from silicon and carbon, the electrical conductivity of silicon increases. More importantly, it significantly compensates for the volume expansion of silicon during application. The porosity of the carbonaceous material increases the stability of the battery by forming a lattice structure to prevent the crushing of silicon [13].

Because of their substantial availability, renewable nature, and affordability, carbon electrode materials produced from biomass have received a great deal of interest nowadays. Additionally, their naturally homogeneous and accurate biological structures can be employed as templates for developing electrode materials with precise and well-defined geometries [14]. Among the numerous types of biomass sources from forestry cultivation production, spruce waste plays an essential role. It is an essential raw material in the cellulose and paper industry. It is used in many areas such as furniture, coating, pencil, and matchstick. Eastern spruce in Turkey has a total area of 334,472 hectares, 230,212 hectares of normal and 104,260 hectares of degraded forest [15]. In the literature, biochar from spruce waste especially respecting biomass-derived biochar-supported Si/C carbonaceous materials are not studied. This study aimed to convert biomass waste into Si-loaded carbonaceous materials with thermochemical and chemical conversion techniques to be evaluated as anode material in supercapacitors and to elucidate their characteristic properties. This present work primarily

focuses on two aspects; *i)* preparation and characterization of carbon-based biochar from spruce waste, and *ii)* comparison of the properties of Si-loaded carbon material produced by chemically activating biochar and biomass.

2 Materials and methods

This section contains information on the materials and experimental details used in the present study.

2.1 Materials

In this section, carbonaceous material production and characterization methods were expressed. The spruce wood sawdust sample (average particle size was 0.75 mm) used as a raw material was collected from a furniture manufacturer near Bursa-Inegöl, which is situated in the Marmara region in western Turkey. In the literature, it has been noted that biomass with high carbon and low ash concentrations provides appropriate precursors for carbonaceous materials [16]. The significant amount of ash and mineral substances in the biomass structure raises the disposal cost and reduces the effectiveness of thermal degradation. The moisture, ash, volatile matter, and fixed carbon contents were 7.46, 1.41, 78.61, and 12.52 wt.%, respectively. The raw material consisted of 46.55 wt.% carbon, 5.16 wt.% hydrogen, 4.56 wt.% nitrogen, and 43.73 wt.% oxygen. The calorific value of the spruce wood sawdust was 19.20 MJ/kg. Lignin, holocellulose, hemicellulose, and extractive contents were 35.21, 54.78, 26.27, and 8.61 wt.%, respectively [17].

2.2 Biochar production

To conduct the pyrolysis tests, a 15 g sample of spruce wood sawdust was put into the reactor and heated at a rate of 10 °C/min to a final temperature of 400–600 °C [18]. This temperature was then sustained for at least 20 min or until no more appreciable gas release was noticed, thereafter the reactor was programmed to cool to ambient temperature. The pyrolysis product yields were gravimetrically calculated by weighing the three products. The liquid product containing aqueous and oil phases was received in cold traps kept at around 0 °C with salty ice, and they were separated and then weighed. The solid product biochar was taken out of the reactor and weighed, and then the gas yield was estimated from the difference to give a total yield of 100%.

2.3 Activation of biomass/biochar with H_3PO_4 and KOH

Biochar obtained from pyrolysis of spruce wood sawdust at a heating rate of 10 °C/min and a temperature of 400 °C was used as a carbonaceous material. Biomass and biochar were activated using two different activating agents (potassium hydroxide (KOH, ≥ 85.0%, Fisher), and phosphoric acid (H_3PO_4, 85 wt.%, Panreac)):

i) In the acidic activation procedure, 15 g of biomass/bio-char was stirred with 300 mL of 1.5 M H_3PO_4 for impregnation. The mixture was stirred at 70 °C for 2 h and dried at 100 °C for 24 h. The activation process was operated at 700 °C in an inert atmosphere of nitrogen for one hour. The prepared activated biochar was maintained at 100 °C for 12 h after being washed with DI water until the pH was roughly neutral.
ii) In the basic activation procedure, 500 ml of 2 M KOH was added to 15 g of biomass/biochar and blended at 70 °C for 2 h. After the filtering step by using the filter paper was finished, it was oven-dried for 24 h at 100 °C. The biomass/biochar was transferred to the steel reactor and placed in the tube furnace, which was increased from room temperature to 700 °C at a heating rate of 10 °C/min. Nitrogen (N_2) gas was used as the sweeping gas in the process, the sample was kept in the furnace at this temperature for 2 h.

These samples obtained from the activation process and named H_3PO_4 or KOH activated biomass/biochar were stocked for use in the silicon loading step. According to the type of raw material and activation agent used in the activation procedure, the coding of the produced activated carbons was as follows: B- for biomass, C- for biochar, -A for H_3PO_4 acid and -B for KOH base. Namely, acid- and base-activated samples of biomass were coded as BA- and BB-, and those of biochar were coded as CA- and CB-, respectively.

2.4 Preparation of Si-loaded carbonaceous materials

The material structure is modified using wet and dry impregnation processes. The precursor solution is employed in the wet impregnation method over the

Table 1 Treatment conditions and sample codes

Treatment Conditions	Sample Code
Biomass + H_3PO_4, 40wt.% Si—550 °C—6 h, air	BA-550–6-A
Biochar + H_3PO_4, 40wt.% Si—600 °C—8 h, air	CA-600–8-A
Biomass + KOH, 40wt.% Si—700 °C—8 h, air	BB-700–8-A
Biochar + KOH, 40wt.% Si—700 °C—8 h, air	CB-700–8-A
Biomass + H_3PO_4, 40wt.% Si—700 °C—8 h, air	BA-700–8-A
Biomass + H_3PO_4, 40wt.% Si—700 °C—8 h, N_2	BA-700–8-N
Biochar + KOH, 40wt.% Si—700 °C—8 h, N_2	CB-700–8-N
Biomass + KOH, 40wt.% Si—700 °C—8 h, N_2	BB-700–8-N

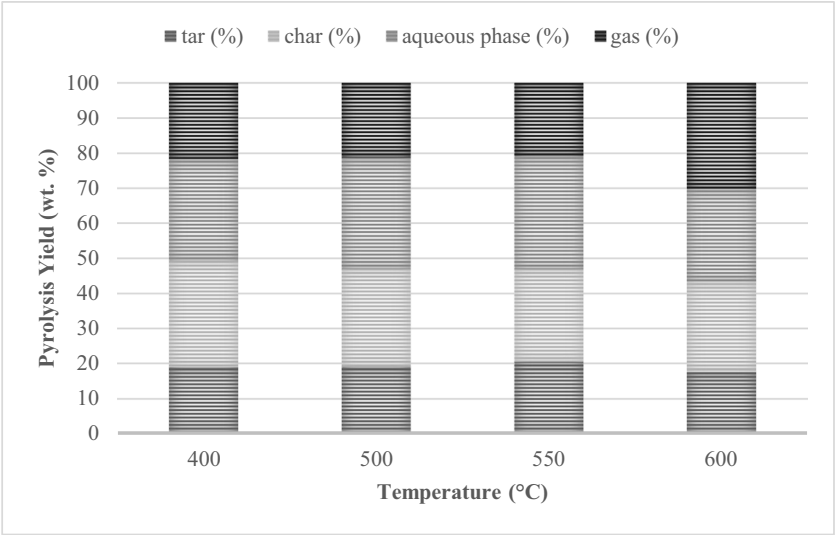

Fig. 1 The pyrolysis product yield of spruce waste at different temperature

Table 2 Elemental analysis results of biomass and biochar samples

	C	H	N	O*	H/C	O/C	N/C
Biomass	46.55	5.16	4.56	43.73	1.33	0.71	0.089
Biochar	85.41	4.20	0.19	10.2	0.59	0.09	0.002

*By the difference

support's pore volume to create a thin slurry. After a specified period has passed, the surplus liquid including any precursors that the support did not retain is separated, the solid is passed through a filter, and the residual solvent in the impregnated support is eliminated by drying. The volume of the solution at the proper amount is equal to or relatively less than the pore volume of the support or other active solid portion in the dry impregnation [19]. The use of dry impregnation reduces the extra liquid used in the wet impregnation method and the requirement for a filtration stage [20]. Activated biomass/biochar supported Si-loaded carbonaceous materials were composed of 40wt.% of Si via dry impregnation of tetraethyl orthosilicate (TEOS, 98%, Acros Organics) as a silicon source. In each step, the carbonaceous material was dried by keeping it in an oven at 105 °C for 30 min and then cooled in a desiccator for 20 min. Si-loaded carbonaceous materials were transferred into a glass reactor and treated using a tubular furnace with a heating rate of 5 °C/min. Treatment conditions including time and temperature were given in Table 1 with sample codes.

In the symbolization, the first part was coded as the type of support material (BA-, BB-, CA-, or CB-), the second part as the temperature (550, 600, or 700 °C), the third part as time (6 or 8 h), and the fourth part as the ambient condition (-A for air and -N for nitrogen).

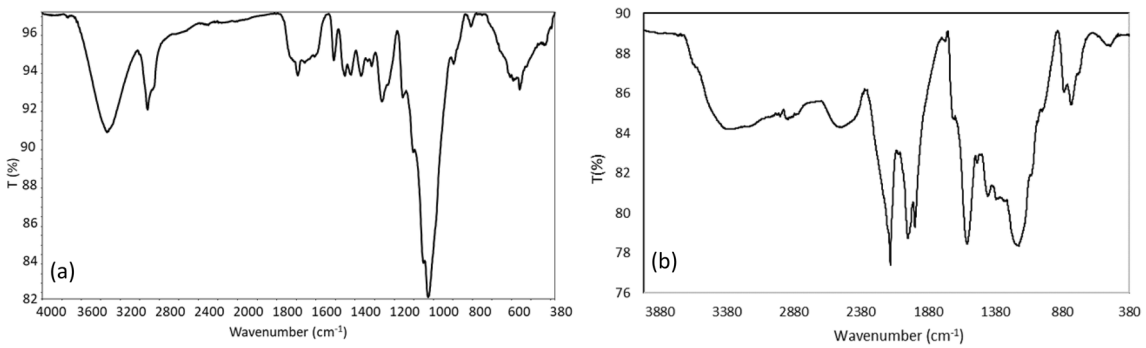

Fig. 2 FT-IR spectrum of (**a**) biomass and (**b**) biochar

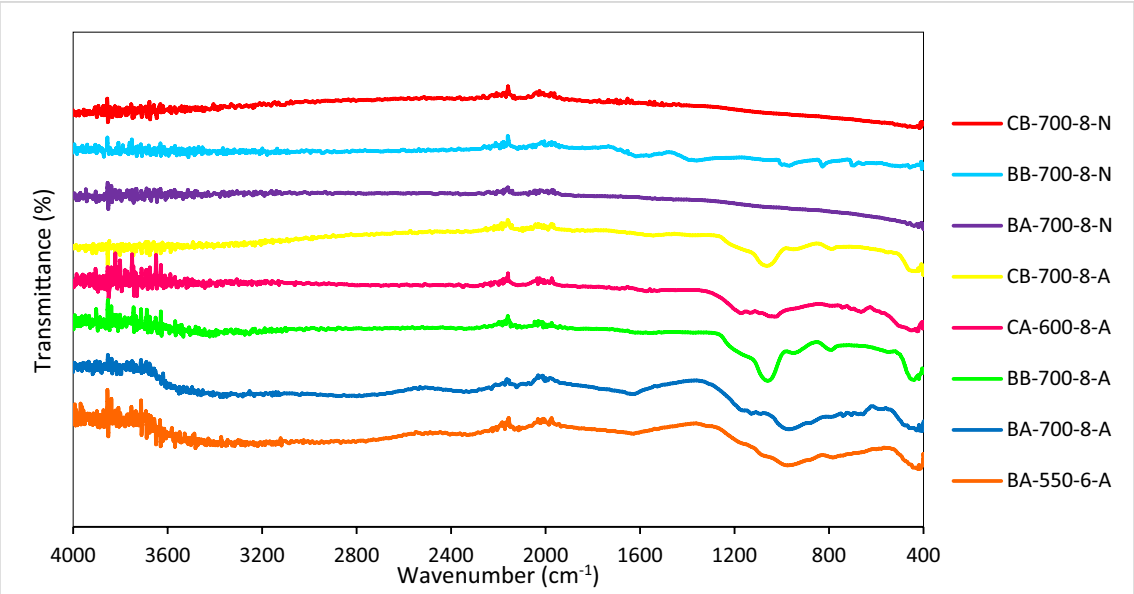

Fig. 3 FT-IR spectrums of Si-loaded carbonaceous materials

2.5 Characterization of biochar and Si-loaded carbonaceous materials

Elemental analysis of biochar was carried out on the Leco CHN628 device. All organic substances were completely combusted by heating the Elemental Analyzer's furnace at 950 °C while implementing helium, dry air, and oxygen gases. FTIR spectra of samples were collected in the 4000–400 cm^{-1} range by using the ATR method to get additional information on the chemical structure of the samples in the near-infrared region (FT-IR, Agilent Cary 630). The surface morphologies of the biochar and Si-loaded carbonaceous materials were detailed using the Scanning Electron Microscope (SEM, ZEISS SUPRA 40VP). Prior to analysis, samples were platinum coated in a Quorum Q300 DC Sputter device under vacuum. The samples' coating thickness after being exposed to the Au/Pd for 1 min was around 100 nm. The 15 kV acceleration voltage (EHT), ~ 10 mm working distance (WD), various magnification ratios, and a secondary electron (SE) detector were the SEM analysis's specifications. XRD analyses of samples were carried out using X-Ray Diffraction Device (XRD, Panalytical-Empyrean) by using CuKα (λ = 0.15405 nm) radiation. X-ray diffraction patterns were obtained at a scanning speed of 2°/min with a 2θ angle range of 5–75°.

Fig. 4 XRD pattern of biochar

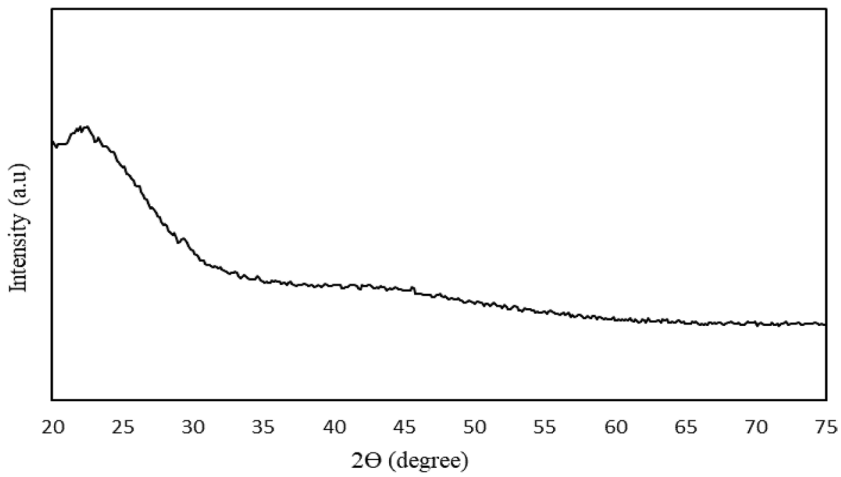

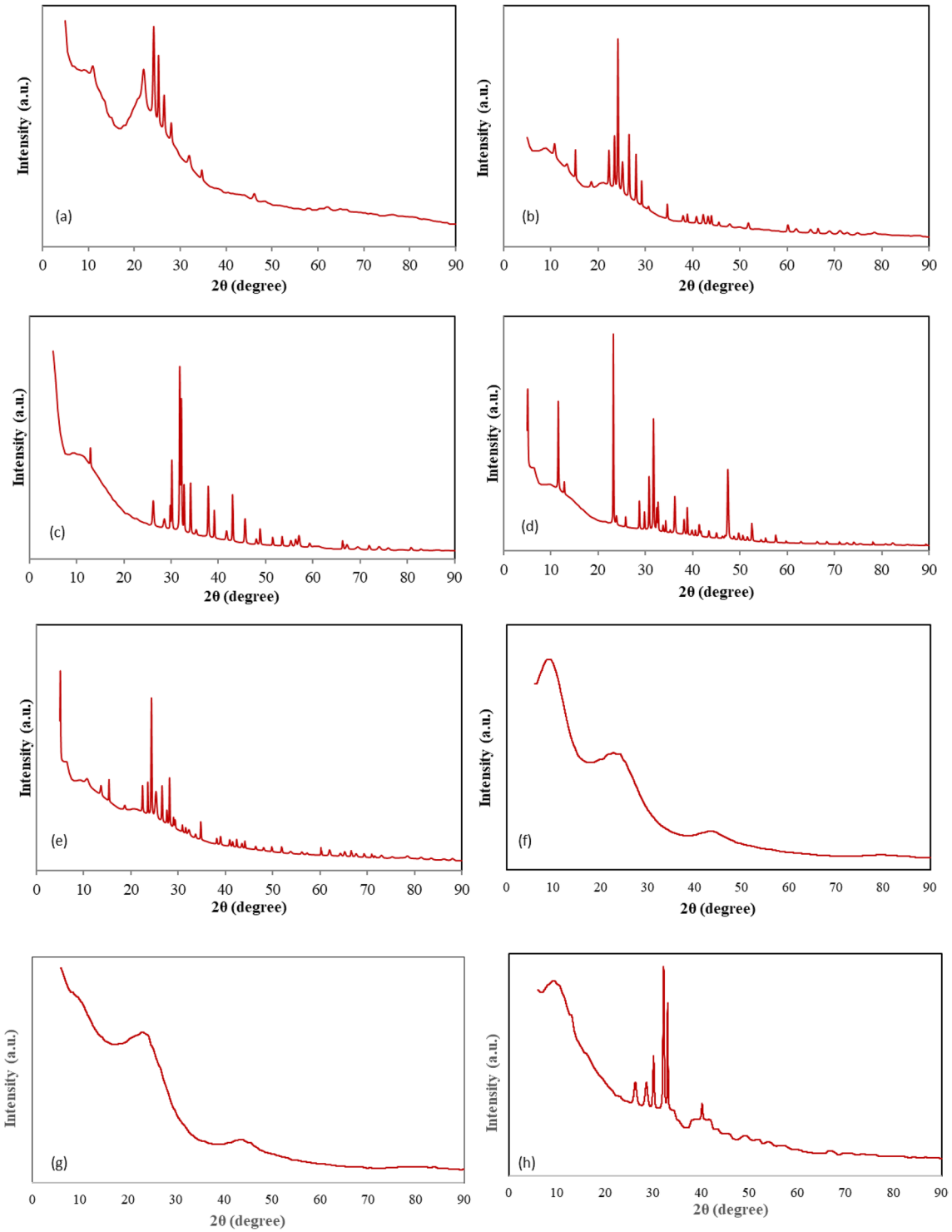

Fig. 5 XRD patterns of (**a**) BA-550–6-A (**b**) CA-600–8-A (**c**) BB-700–8-A (**d**) CB-700–8-A (**e**) BA-700–8-A (**f**) BA-700–8-N (**g**) CB-700–8-N (**h**) BB-700–8-N

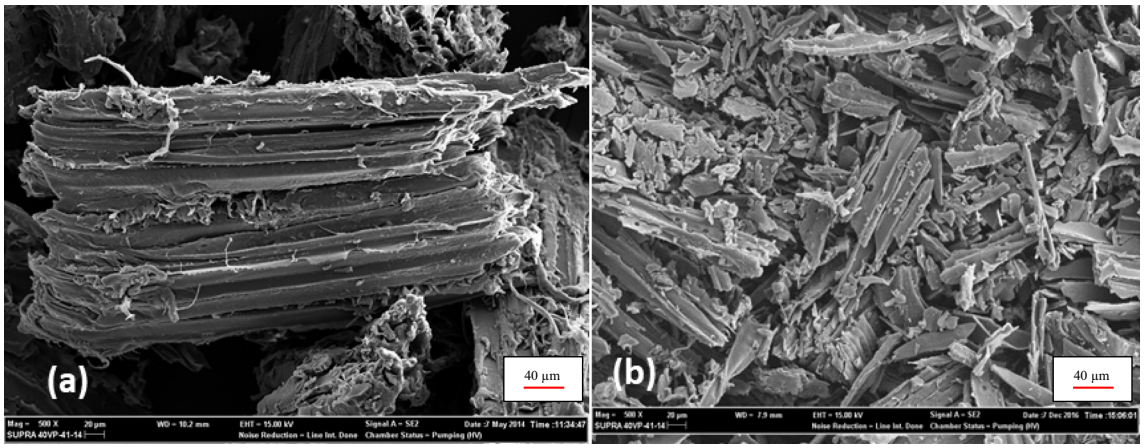

Fig. 6 SEM images of (**a**) biomass and (**b**) biochar (500 x)

3 Results and discussion

The results obtained from the experimental studies were given in detail under this section.

3.1 Comparison of the pyrolysis products yields

The pyrolysis of the spruce waste was performed in a fixed-bed reactor under a static medium with a heating rate of 10 °C/min, and experimental details were given in our previous study [21]. Figure 1 showed the impact of temperature on the yields of pyrolysis products. When the pyrolysis temperature was changed between 400–600 °C, the maximum tar yield of 20.50% was reached at 550 °C. It was determined that the biochar yield reduced with rising temperature. The highest char yield (30.25%) was obtained at 400 °C. The solid byproduct that occurred after pyrolysis was referred to as "char" and was made up of organic material with degradation ranging from insufficiently pyrolyzed biomass at low temperatures to a greatly carbonized material at high temperatures. The char also contained any coke that could have been produced due to the reactions between the volatile compounds [22]. Because of the fast oxidation of spruce sawdust waste and char in the entity of oxygen over 550 °C, the char yield became relatively minimal. In this study, the solid product obtained from 400 °C was used in the production of the material to be used as Si-loaded carbonaceous materials.

3.2 Characterization of carbonaceous materials

Biomass, biochar, and Si-loaded materials could be characterized by employing a variety of analytical techniques to determine their potential use as adsorbents for trace elements from water [23], solid fuels [24], composite material for adsorption of Cu(II) [25], etc. In this study biochar and Si-loaded materials were characterized to investigate if they could be used as carbonaceous materials. FT-IR, SEM, XRD, and elemental analysis results of all materials were given in this section.

3.2.1 Elemental analysis

Elemental analysis results of the spruce waste and biochar obtained at 400 °C pyrolysis temperature was given in Table 2. H/C and O/C atomic ratios were crucial components to fuel [26]. As investigation criteria for the specific properties and structures of biomass, such as aromaticity and functionality, the composition of C, H, and O or the H/C and O/C ratios were frequently utilized. Table 2 also showed the relevance between the H/C and O/C ratio of the biomass and biochar. The atomic ratio could be defined by the C, H, N, and O weight percentages. The fact that the decrease in H/C and O/C ratios indicated a loss of hydrogen and oxygen, besides a gradual rise of char with carbon.

According to elemental analysis results, when the carbon content of biochar from spruce wood sawdust was compared with feedstock, it was observed that char had higher carbon content than the biomass. In addition, the N/C ratio is a measure of the characteristics of the biomass sample, similar to the O/C and H/C ratios [27]. It indicates the role of biomass as a soil nutrient [28] and is typically not considerably influenced by temperature [27].

3.2.2 Fourier transform infrared spectroscopy analysis

FT-IR spectrums of biomass, biochar and Si-loaded materials were given in Figs. 2 and 3, respectively. Bands caused by ambient CO_2 contributions have been eliminated from the spectra to enhance the spectral quality. When compared to FT-IR spectra of biochar and the Si-loaded materials obtained from different

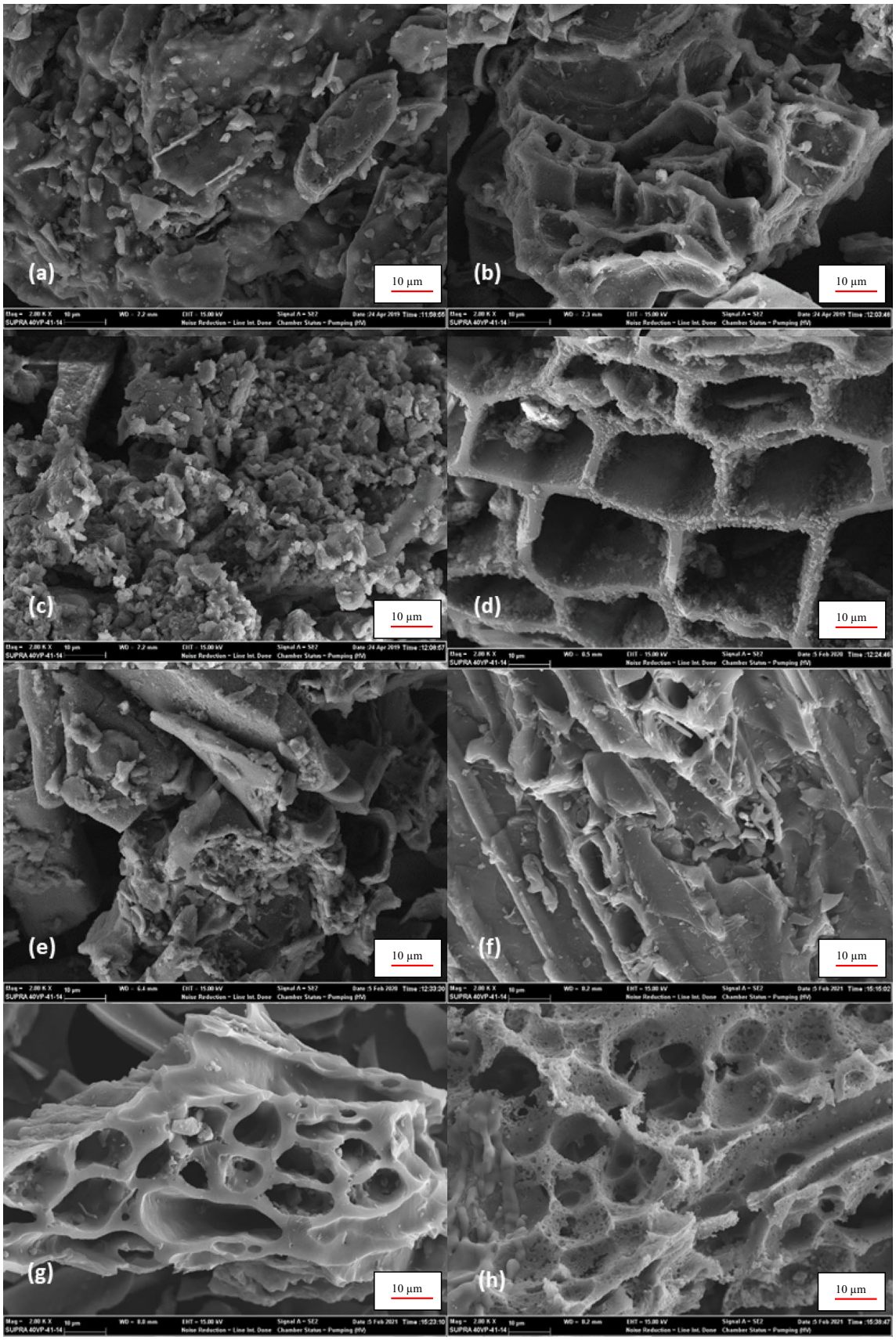

Fig. 7 SEM images of (**a**) BA-550–6-A (**b**) CA-600–8-A (**c**) BB-700–8-A (**d**) CB-700–8-A (**e**) BA-700–8-A (**f**) BA-700–8-N (**g**) CB-700–8-N (**h**) BB-700–8-N

Table 3 Elemental composition of Si-loaded carbonaceous materials from EDX analysis

	Si (wt.%)	C (wt.%)	O (wt.%)	P (wt.%)	K (wt.%)
BA-550–6-A	27.43	8.28	46.91	17.38	-
CA-600–8-A	10.33	41.78	38.42	9.47	-
BB-700–8-A	19.61	33.45	46.95	-	-
CB-700–8-A	26.65	25.25	48.10	-	-
BA-700–8-A	18.15	13.22	51.56	17.06	-
BA-700–8-N	20.83	51.24	27.94	-	-
CB-700–8-N	0.18	78.98	20.84	-	-
BB-700–8-N	0.58	49.19	29.55	-	20.68

activation processes, significant modifications were noted in the chemical structure of the sample. The spectra of biomass, biochar, BA-550–6-A, and BA-700–8-A all showed a high-strong peak at about 3400 cm^{-1}, and this peak was generated by stretching vibrations of the O–H bonds in hydroxyl groups. Methyl and methylene groups' asymmetric and symmetric vibration frequencies at 2918 cm^{-1} and 2850 cm^{-1} were observed in the biomass's spectrum; however, the peak was not seen in the spectra of the Si-loaded carbonaceous materials because of the activation process. Biochar lacked the symmetric stretching vibration at around 2850 cm^{-1} [29] and the asymmetric stretching vibration at about 2900 cm^{-1} of the C-H bonds that were present in biomass [30]. As evidenced by the observation of C = C bonds at 1570 cm^{-1} for biochar, it was likely that the C-H bonds were broken during the thermochemical conversion process to create more durable C = C bonds [31]. Additionally, because oxygenated groups on the surface were changed to CO and CO_2 during decomposition [32], the C = O stretching band detected at 1720 cm^{-1} in the biomass was not present in the biochar [33]. The peak at ~ 1600 cm^{-1} was attributable to vibrations of the C = O groups in aldehydes and ketones and this peak appeared in the spectra of all samples. The shoulder was seen at 1240 cm^{-1} in the Si-loaded samples treated in a nitrogen atmosphere, and the spectra of the aforesaid carbonaceous materials contained a band at 1110 cm^{-1} that was attributed to Si–O-Si vibrations, it was evident that silicon was loaded. The peak at around 680 and 470 cm^{-1} attributed to the existence of S–H groups [34]. The presence of Si–O, and Si–O-Si peaks in the FTIR spectrums revealed the existence of SiO_2 formation in the silicon particles loaded on the activated biomass and biochar. The nature of readily oxidizing silicon particles can be linked to this scenario [35]. The FT-IR spectra were consistent with the patterns of Si-loaded carbon materials in the literature. In addition, it was determined that FT-IR spectra and XRD results confirmed each other.

3.2.3 X-ray diffraction analysis

X-ray diffraction patterns of biochar and Si-loaded carbonaceous materials produced as a result of the activation of biomass or biochar with two different chemical activation agents were given in Figs. 4 and 5, respectively. The characteristic peaks in XRD patterns of Si-doped biomass-based materials were specified by crosschecking with the JCPDS (Joint Committee on Powder Diffraction Standards) card numbers 96–101-1061, 96–110-1022, 96–901-2706/6404, 98–001-6611, 98–002-8347/4259, 98–007-9698/5302, 98–008-8811, 98–015-5250, 98–016-2629, 98–017-2292, 98–018-0567/0900/0563, and 98–064-1278. As seen in Fig. 4, the biochar had an amorphous structure.

Due to the XRD pattern of BA-550–6-A, the wide peak in the range of 2θ = 0°-30° indicated the amorphous structure, and the peak at 2θ = 25° demonstrated the crystalline structures in the material. In the XRD pattern, the peaks around 24°, 28° and 34° indicated the presence of tetragonal cristobalite alpha (SiO_2), and the peaks around 26° and 46° represented the existence of hexagonal graphite structure. In the XRD pattern of CA-600–8-A, the wide peak between 2θ values of 20° and 30° proved the presence of an amorphous structure. High-intensity peaks observed at 2θ = 24°, 25°, 26°, and 29° indicated that the crystallinity of the CA-600–8-A sample had increased compared to the BA-550–6-A. In XRD pattern, the peaks at 24°, 28°-30°, 37°-40°, 43°, 47°-78° demonstrated the presence of the structure of monoclinic cristobalite (SiO_2) and monoclinic coesite (SiO_2), and the peak around 26° was hexagonal graphite. The XRD result of the carbonaceous material obtained as a result of heating of the 40wt.% Si-loaded sample at 700 °C for 8 h after the treatment of the biomass with KOH (BB-700–8-A) showed that the treatment conditions provided the best crystal structure. In the XRD pattern, peaks around 31°, 37°, 56° and 66° indicated the presence of hexagonal SiO_2, while peaks around 26° specified the entity of hexagonal graphite structure. When the XRD results of BB-700–8-A and CB-700–8-A materials were compared; it was concluded that the carbonaceous material obtained when the activation process with KOH was performed had a better crystal structure than the material activated with H_3PO_4. In the XRD pattern, peaks indicating the presence of tetragonal cristobalite (SiO_2) and monoclinic coesite (SiO_2) (2θ = 23°, 32°-33°, 38°, 40°, 41°, 45°, 47°, 50°, 54°, 66°, 68°, 74°, 78°, and 85°), and also orthorhombic graphite (2θ = 31°, 33°, 41°, 46°, 51°, 55°, 62°, 66°, and 72°) structures were detected. When the XRD result of BA-700–8-A was compared with that of BA-550–6-A, it was concluded that the crystalline structure was improved by increasing the activation temperature. In the XRD pattern, peaks indicating the presence of tetragonal cristobalite (SiO_2) and monoclinic coesite

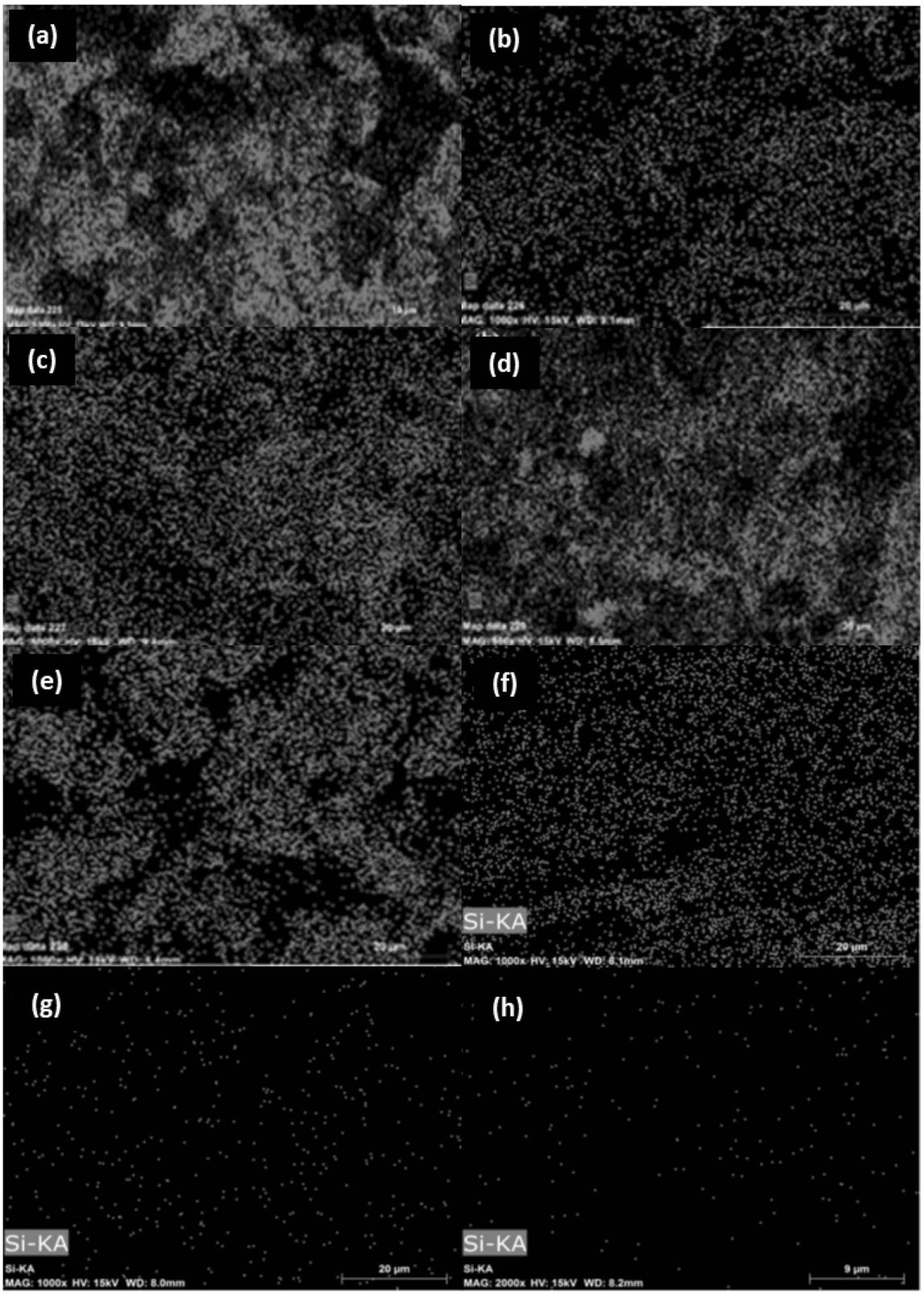

Fig. 8 The distribution of Si on the carbonaceous materials (**a**) BA-550–6-A (**b**) CA-600–8-A (**c**) BB-700–8-A (**d**) CB-700–8-A (**e**) BA-700–8-A (**f**) BA-700–8-N (**g**) CB-700–8-N (**h**) BB-700–8-N

(SiO_2) (2θ = 13°, 22°, 24°-25°, 28°-29°, 32°, 38°, 41°, 44°, 48°-49°, 60°, 66°, 69°-70°, 75°, and 81°-83°), and also hexagonal graphite (2θ = 26°, 43°, and 46°) structures were assigned. The XRD patterns of the test results carried out to examine the influence of the heating medium on the high-temperature treatment of biomass or biochar were given in Fig. 4 (f–h) for BA-700–8-N, CB-700–8-N, and BB-700–8-N. When XRD patterns were compared, it was seen that crystal structures could not be obtained in BA-700–8-N and CB-700–8-N where the materials were in an amorphous structure. In the XRD pattern of BB-700–8-N, the formation of K_2O structures in cubic crystal form on the sample due to the activation of the biomass with KOH was determined with the peaks detected around 26° and 30°. In the XRD pattern, the peaks around 28°, 32°, 33°, and 40° displayed the presence of an anorthic (Si) crystal structure.

3.2.4 Scanning electron microscopy analysis

The surface morphology of biomass and biochar was given in Fig. 6. Both spruce tree sawdust and the biochar had a fibrous morphology; the biochar had also smaller particle sizes in similar magnification (500 x). SEM images of Si-loaded carbonaceous materials were given in Fig. 7. The SEM images of Si-loaded carbonaceous materials (BA-550–6-A, CA-600–8-A, BA-700–8-A) obtained by the activation of biomass or biochar with H_3PO_4 exhibited a denser and smoother surface. The reason for this situation was the accumulation of phosphorus in the H_3PO_4 structure that forms in the pores and covers them as a result of the acid activation treatment. On the other hand, carbonaceous materials prepared with KOH (BB-700–8-A, CB-700–8-A) had porous structures, because leaving the activating agents from the structure resulted in the open spaces that were previously occupied by them. In addition, the activating substances decomposed at higher temperatures, resulting in the formation of a porous texture due to the combustion of the carbon structure. As seen in the SEM image of BB-700–8-N which was activated with KOH, the carbonaceous material had a foamy structure.

EDX analyses results of Si-loaded carbonaceous materials were given in Table 3. The distribution of Si was also specified by EDX-mapping analyses (Fig. 8). As seen in Table 3, the Si element was detected by EDX analysis, and the highest silicon content of 27.43wt.% was obtained in BA-550–6-A material. This was followed by 26.65wt.% for CB-700–8-A. Si loading was not successfully performed in CB-700–8-N, potassium remaining after the activation process in the biomass structure was determined as 20.68% by weight for BB-700–8-N. When the silicon distributions obtained by elemental mapping were examined, it was seen that the silicon had a homogeneous distribution on the support materials' surface, which showed that the silicon was successfully loaded (Fig. 8). Si-structures detected in XRD and FT-IR analyses were also seen homogeneously distributed on the surface in SEM–EDX-mapping analysis. The results obtained from these different analyzes were in the harmony with each other. Wang et al. [36] investigated the characteristics of porous activated carbon micro sheets derived from pomelo peel by doping with nitrogen and phosphorus, and it was reported that effective doping was achieved by providing homogeneous distribution as a result of the elemental mapping, similar to this study. When Hasegawa et al. [37] added Si nanoparticles to the porous carbon monolith produced from resorcinol–formaldehyde resin and tested it as a free-standing electrode for Li-ion batteries, the EDX mapping result showed that the Si molecules were distributed uniformly throughout the entire monolith.

4 Conclusion

In the study, spruce wood sawdust was chosen as the raw material for the production of Si-doped biomass-based materials. The sawmill waste, which contained 46.55 wt.%, was suitable for use in the production of carbonaceous materials. In addition, spruce wood sawdust was also an appropriate raw material for biomass conversion by thermochemical processes with 78.61 wt.% volatile matter content. Support material type, activation, and doping conditions were changed to determine the effect of these parameters on the physicochemical properties of the obtained carbonaceous material. According to the FTIR results, the Si–O-Si vibration in the spectrums showed that the silicon had been successfully loaded into the support material. EDX-mapping results also confirmed the Si distribution was homogenous onto the surface of the materials. According to the XRD results, it was seen that the amorphous structure of biochar was preserved in each sample synthesized. Different crystalline phases of Si were detected in the samples apart from the samples heated at 700 °C for 8 h. Synthesis of Si-doped carbonaceous material from spruce wood sawdust with thermochemical methods and using these porous materials in lithium-ion battery applications was a promising result for evaluating biomass and biochar in a different application area. This study should be evaluated as an optimization study. The experimental results obtained from this study will light the way for future laboratory and pilot-scale experiments to be tested in battery applications.

Authors' contributions NO: conceptualization. ASY and EY: methodology, writing, data curation. RZY: investigation. KBD and ST: review and editing.

Funding Financial assistance 2018–02.BŞEÜ.03–01 project number received from Bilecik Şeyh Edebali University Scientific Research Council.

Data availability Not applicable.

Declarations

Ethical approval Not applicable.

Competing interests The authors declare no competing interests.

References

1. Seow YX, Tan YH, Mubarak NM, Kansedo J, Khalid M, Ibrahim ML, Ghasemi M (2022) A review on biochar production from different biomass wastes by recent carbonization technologies and its sustainable applications. J Environ Chem Eng 10:107017. https://doi.org/10.1016/j.jece.2021.107017
2. Yaman E (2023) Influence of catalyst support type on silver poplar pyrolysis vapors: a Py/GC-MS study. J Porous Mater 1–12. https://doi.org/10.1007/s10934-023-01435-1
3. Van Ommen JR, de Jong W (2014) Biomass as a sustainable energy source for the future: fundamentals of conversion processes. Wiley, USA
4. Neogi S, Sharma V, Khan N, Chaurasia D, Ahmad A, Chauhan S, Bhargava PC (2021) Sustainable biochar: a facile strategy for soil and environmental restoration, energygeneration, mitigation of global climate change and circular bioeconomy. Chemosphere 293:133474. https://doi.org/10.1016/j.chemosphere.2021.133474
5. Ma ZW, Liu HQ, Lü QF (2021) Porous biochar derived from tea saponin for supercapacitor electrode: Effect of preparation technique. J of Energy Storage 40:102773. https://doi.org/10.1016/j.est.2021.102773
6. Villota SM, Lei H, Villota E, Qian M, Lavarias J, Taylan V, Agulto I, Mateo W, Valentin M, Denson M (2019) Microwave-assisted activation of waste cocoa pod husk by H3PO4 and KOH—comparative insight into textural properties and pore development. ACS Omega 4(4):7088–7095. https://doi.org/10.1021/acsomega.8b03514
7. Prauchner MJ, Rodríguez-Reinoso F (2012) Chemical versus physical activation of coconut shell: A comparative study. Microporous Mesoporous Mater 152:163–171. https://doi.org/10.1016/j.micromeso.2011.11.040
8. Shamsuddin MS, Yusoff NRN, Sulaiman MA (2016) Synthesis and characterization of activated carbon produced from kenaf core fiber using H_3PO_4 activation. Procedia Chem 19:558–565. https://doi.org/10.1016/j.proche.2016.03.053
9. Norouzi O, Jafarian S, Safari F, Tavasoli A, Nejati B (2016) Promotion of hydrogen-rich gas and phenolic-rich bio-oil production from green macroalgae Cladophora glomerata via pyrolysis over its bio-char. Bioresour Technol 219:643–651. https://doi.org/10.1016/j.biortech.2016.08.017
10. Norouzi O, Salimi P, Maria FD, Pourhosseini SEM, Safari F (2019) Synthesis and design of engineered biochars as electrode materials in energy storage systems. In: Zhen F, Richard LS, Xiao-Fei T (eds) Production of Materials from Sustainable Biomass Resources. Springer, Singapore, pp 233–265
11. Wang Y, Jiang M, Yang Y, Ran F (2016) Hybrid electrode material of vanadium nitride and carbon fiber with cigarette butt/metal ions wastes as the precursor for supercapacitors. Electrochim Acta 222:1914–1921. https://doi.org/10.1016/j.electacta.2016.12.003
12. Hu L, Jin M, Zhang Z, Chen H, Boorboor Ajdari F, Song J (2022) Interface-adaptive binder enabled by supramolecular interactions for high-capacity Si/C composite anodes in lithium-ion batteries. Adv Funct Mater 32:2111560. https://doi.org/10.1002/adfm.202111560
13. Ji H, Chen Q, Hua K, Ma Q, Wang R, Zhang L, Zhang C (2022) Si nanoparticles embedded in porous N-doped carbon fibers as a binder-free and flexible anode for high-performance lithium-ion batteries. J Alloys Compd 936:168256. https://doi.org/10.1016/j.jallcom.2022.168256
14. Manasa P, Sambasivam S, Ran F (2022) Recent progress on biomass waste derived activated carbon electrode materials for supercapacitors applications—A review. J Energy Storage 54:105290. https://doi.org/10.1016/j.est.2022.105290
15. Gönültas O, Uçar M (2019) Utilization of bark tannins from oriental spruce and oak in bioadhesive production. Turk J For 20:458–465
16. Köseoğlu E, Akmil-Başar C (2015) Preparation, structural evaluation and adsorptive properties of activated carbon from agricultural waste biomass. Adv Powder Technol 26(3):811–818. https://doi.org/10.1016/j.apt.2015.02.006
17. Ozbay N, Yargic AS (2019) Carbon foam production from bio-based polyols of liquefied spruce tree sawdust: Effects of biomass/solvent mass ratio and pyrolytic oil addition. J Appl Polym Sci 136:47185. https://doi.org/10.1002/app.47185
18. Yargic AS (2021) Conversion of biopitch to carbon foam with tunable properties: The role of chemical activation. In: Kavak D (ed) Current engineering sciences research, 1st edn. Livre de Lyon, France, pp 1–21
19. Campanati M, Fornasari G, Vaccari A (2003) Fundamentals in the preparation of heterogeneous catalysts. Catal Today 77(4):299–314. https://doi.org/10.1016/S0920-5861(02)00375-9
20. Mehrabadi BA, Eskandari S, Khan U, White RD, Regalbuto JR (2017) A review of preparation methods for supported metal catalysts. Adv Catal 61:1–35. https://doi.org/10.1016/bs.acat.2017.10.001
21. Ozbay N, Yargic AS, Sahin RZY, Yaman E (2019) Valorization of banana peel waste via in-situ catalytic pyrolysis using Al-Modified SBA-15. Renew Energ 140:633–646. https://doi.org/10.1016/j.renene.2019.03.071
22. Sharma RK, Hajaligol MR, Martoglio Smith PA, Wooten JB, Baliga V (2000) Characterization of char from pyrolysis of chlorogenic acid. Energ Fuels 14(5):1083–1093. https://doi.org/10.1021/ef000058z
23. Hamid Y, Liu L, Usman M, Naidu R, Haris M, Lin Q, Yang X (2022) Functionalized biochars: synthesis, characterization, and applications for removing trace elements from water. J Hazard Mater 437:129337. https://doi.org/10.1016/j.jhazmat.2022.129337
24. Mukhambet Y, Shah D, Tatkeyeva G, Sarbassov Y (2022) Slow pyrolysis of flax straw biomass produced in Kazakhstan: Characterization of enhanced tar and high-quality biochar. Fuel 324:124676. https://doi.org/10.1016/j.fuel.2022.124676
25. Liu J, Liu H, Yang X, Jia X, Cai M, Bao Y (2021) Preparation of Si–Mn/biochar composite and discussions about characterizations, advances in application and adsorption mechanisms. Chemosphere 281:130946. https://doi.org/10.1016/j.chemosphere.2021.130946
26. Gan YY, Ong HC, Show PL, Ling TC, Chen WH, Yu KL, Abdullah R (2018) Torrefaction of microalgal biochar as potential coal fuel and application as bio-adsorbent. Energy Convers Manag 165:152–162. https://doi.org/10.1016/j.enconman.2018.03.046
27. Liu L, Tan Z, Gong H, Huang Q (2018) Migration and transformation mechanisms of nutrient elements (N, P, K) within biochar in straw–biochar–soil–plant systems: a review. ACS Sustain Chem Eng 7:22–32. https://doi.org/10.1021/acssuschemeng.8b04253
28. Qin F, Zhang C, Zeng G, Huang D, Tan X, Duan A (2022) Lignocellulosic biomass carbonization for biochar production and characterization of biochar reactivity. Renew Sustain Energy Rev 157:112056. https://doi.org/10.1016/j.rser.2021.112056
29. Awe AA, Opeolu BO, Fatoki OS, Ayanda OS, Jackson VA, Snyman R (2020) Preparation and characterisation of activated carbon

from Vitis vinifera leaf litter and its adsorption performance for aqueous phenanthrene. Appl Biol Chem 63:1–17. https://doi.org/10.1186/s13765-020-00494-1
30. Correa CR, Otto T, Kruse A (2017) Influence of the biomass components on the pore formation of activated carbon. Biomass Bioenerg 97:53–64. https://doi.org/10.1016/j.biombioe.2016.12.017
31. Dodevski V, Janković B, Stojmenović M, Krstić S, Popović J, Pagnacco MC, Pašalić S (2017) Plane tree seed biomass used for preparation of activated carbons (AC) derived from pyrolysis; Modeling the activation process. Colloids Surf A: Physicochem Eng Aspects 522:83–96. https://doi.org/10.1016/j.colsurfa.2017.03.003
32. Lawal IA, Chetty D, Akpotu SO, Moodley B (2017) Sorption of Congo red and reactive blue on biomass and activated carbon derived from biomass modified by ionic liquid. Environ Nanotechnol 8:83–91. https://doi.org/10.1016/j.enmm.2017.05.003
33. Sun Y, Li H, Li G, Gao B, Yue Q, Li X (2016) Characterization and ciprofloxacin adsorption properties of activated carbons prepared from biomass wastes by H_3PO_4 activation. Bioresour Technol 217:239–244. https://doi.org/10.1016/j.biortech.2016.03.047
34. Cuong DV, Wu PC, Liu NL, Hou CH (2020) Hierarchical porous carbon derived from activated biochar as an eco-friendly electrode for the electrosorption of inorganic ions. Sep Purif Technol 242:116813. https://doi.org/10.1016/j.seppur.2020.116813
35. Hatipoglu G, Alaf M, Akbulut H (2019) Electrochemical performances of graphene and MWCNT supported metallurgical grade silicon anodes. J Mater Sci: Mater Electron 30:2067–2079. https://doi.org/10.1007/s10854-018-0478-y
36. Wang Z, Tan Y, Yang Y, Zhao X, Liu Y, Niu L, Tichnell B, Kong L, Kang L, Liu Z, Ran F (2018) Pomelo peels-derived porous activated carbon microsheets dual-doped with nitrogen and phosphorus for high performance electrochemical capacitors. J Power Sources 378:499–510. https://doi.org/10.1016/j.jpowsour.2017.12.076
37. Hasegawa G, Kanamori K, Nakanishi K, Hayashi K (2019) Thermogravimetric evolved gas analysis and microscopic elemental mapping of the solid electrolyte interphase on silicon incorporated in free-standing porous carbon electrodes. Langmuir 35(39):12680–12688. https://doi.org/10.1021/acs.langmuir.9b02085